International Journal of Peptide Research and Therapeutics (2026) 32:30
https://doi.org/10.1007/s10989-026-10810-w

Brain Delivery of a Kv1.3-Blocking Peptide is not Enhanced by Conjugation to Blood–Brain Barrier Shuttle Peptides

Dorothy C. C. Wai[1] · Liam M. Koehn[2] · Ethan Kreutzer[2] · Pranav Runwal[2] · Muhammad Umair Naseem[3] · Gyorgy Panyi[3] · David I. Finkelstein[4] · Joseph A. Nicolazzo[2,5] · Raymond S. Norton[1]

Received: 13 December 2025 / Accepted: 1 February 2026

Abstract

Purpose The voltage-gated potassium channel $K_V1.3$ is upregulated on pro-inflammatory microglia, and its blockade is effective in reducing neuroinflammation in vitro and in vivo. The most potent and selective $K_V1.3$ blockers identified to date are disulfide-rich, venom-derived peptides, which are largely excluded from the brain by the blood–brain barrier (BBB). As BBB shuttle peptides have been reported to promote receptor-mediated transport of macromolecules and nanoparticles across the BBB, we have conjugated two such shuttle peptides, MTfpep (MTf) and Angiopep-2 (Ang2), to HsTX1[R14A], a $K_V1.3$-blocking peptide with 34 residues and four disulfide bonds, using click chemistry.

Results NMR spectroscopy showed that the conjugates adopted the same fold as HsTX1[R14A], and electrophysiology assays demonstrated the retention of nanomolar $K_V1.3$ inhibition. Liquid chromatography tandem mass spectrometry (LC-MS/MS) assays were developed to quantify HsTX1[R14A] and MTf-HsTX1[R14A] in buffer, mouse plasma and brain homogenate; however, sufficient analytical sensitivity could not be achieved for Ang2-HsTX1[R14A]. Assessment of peptide permeability in in vitro BBB models showed no evidence of enhanced permeability of MTf-HsTX1[R14A] relative to HsTX1[R14A]. Following intravenous administration of MTf-HsTX1[R14A] to C57BL/6 mice at 4 mg/kg, plasma concentrations were detectable up to 120 min post-dose, but brain concentrations of MTf-HsTX1[R14A] remained below the limit of detection at all timepoints measured.

Conclusion Our results imply that the BBB shuttle peptide MTfpep failed to facilitate brain entry of this cargo. Nevertheless, the click chemistry methods developed for HsTX1[R14A] will facilitate its modular assembly with other brain-targeting ligands and are applicable to conjugation of other disulfide-rich peptides.

Keywords Disulfide-rich peptides · $K_V1.3$ · Click chemistry · Brain delivery · Blood–brain barrier · MTfpep

Abbreviations

ACN	Acetonitrile
AD	Alzheimer's disease
BBB	Blood–brain barrier
DMF	N,N-Dimethylformamide
CNS	Central nervous system
CuAAC	Copper-catalyzed azide–alkyne cycloaddition
FBS	Foetal bovine serum

Dorothy C. C. Wai and Liam M. Koehn contributed equally to this work.

✉ Raymond S. Norton
ray.norton@monash.edu

[1] Medicinal Chemistry, Monash Institute of Pharmaceutical Sciences, Monash University, 381 Royal Parade, Parkville, VIC 3052, Australia

[2] Drug Delivery, Disposition and Dynamics, Monash Institute of Pharmaceutical Sciences, Monash University, Parkville, VIC 3052, Australia

[3] Department of Biophysics and Cell Biology, Faculty of Medicine, University of Debrecen, Debrecen 4032, Hungary

[4] Parkinson's Disease Laboratory, Florey Institute of Neuroscience and Mental Health, The University of Melbourne, Parkville, VIC 3010, Australia

[5] Centre for Drug Candidate Optimisation, Monash Institute of Pharmaceutical Sciences, Monash University, Parkville, VIC 3052, Australia

Published online: 15 February 2026

Fmoc	Fluorenylmethyloxycarbonyl
HCTU	O-(1 H-6-Chlorobenzotriazole-1-yl)-1,1,3,3-tetramethyluronium hexafluorophosphate
i.v.	Intravenous
LC-MS	Liquid chromatography mass spectrometry
LLQ	Lower limit of quantification
LPS	Lipopolysaccharide
LRP-1	Low-density lipoprotein receptor-related protein 1
NMR	Nuclear magnetic resonance
PD	Parkinson's disease
PEG	Polyethylene glycol
RP-HPLC	Reversed-phase high-performance liquid chromatography
s.c.	Subcutaneous
TEA	Tetraethylammonium
TFA	Trifluoroacetic acid
THPTA	Tris(3-hydroxypropyltriazolylmethyl)amine

Introduction

Effective therapies for neurodegenerative diseases such as Alzheimer's disease (AD) and Parkinson's disease (PD) are limited. There is growing recognition of neuroinflammation as a common pathological mechanism with the potential to be addressed by next-generation therapeutics (Heneka et al. 2025; Tansey et al. 2022; Zhang et al. 2023). However, drug access to the brain parenchyma from the systemic circulation is limited by the blood–brain barrier (BBB), which is formed by the vascular endothelium in the brain connected by tight junctions. A key challenge for molecules targeting the central nervous system (CNS) is therefore the delivery of efficacious drug concentrations into the brain following peripheral administration.

The voltage-gated potassium channel $K_V1.3$ is a promising target in neurodegenerative diseases that is upregulated in both AD and PD postmortem human brains and animal models (Rangaraju et al. 2015; Sarkar et al. 2020), as well as in mice that have been challenged with lipopolysaccharide (LPS) (Di Lucente et al. 2018). $K_V1.3$ is essential for the activation of pro-inflammatory microglia (Di Lucente et al. 2018), and its blockade has been shown to be therapeutically beneficial in mouse models of AD and PD (Maezawa et al. 2017; Sarkar et al. 2020). These studies utilized PAP-1, a small-molecule $K_V1.3$ inhibitor that is brain-penetrant but has modest $K_V1.3$ activity (~2 nM) and selectivity (~25-fold) (Schmitz et al. 2005). In contrast, venom-derived $K_V1.3$-blocking peptides typically display superior target selectivity, owing to a larger interaction surface area with the channel that includes contact with residues further away from the K^+-conducting pore, which are less conserved between K_V1 family members (Norton and Chandy 2017).

HsTX1[R14A], an analogue of the peptide toxin HsTX1 from the scorpion *Heterometrus spinifer*, is a highly potent (IC_{50}~45 pM) $K_V1.3$-blocking peptide that is >2000-fold selective for $K_V1.3$ over other K_V1 channels (Lebrun et al. 1997; Rashid et al. 2014). It contains 34 residues and four disulfide bridges (Fig. 1), which impart exceptional chemical, proteolytic and plasma stability (Jin et al. 2016; Rashid et al. 2014). We have shown that peripherally-administered HsTX1[R14A] improved cognitive function in a SAMP8 mouse model of sporadic AD (Pan et al. 2023), and reduced markers of neuroinflammation in mice challenged with LPS (Reddiar et al. 2021). Similarly, another peptidic $K_V1.3$ inhibitor, ShK-233, improved cognitive function in a 5xFAD mouse model of familial AD (Ramesha et al. 2021). The beneficial effects of these relatively large peptides might be attributable to disruption of the BBB associated with disease progression in these models (also reflected in human AD), which could allow greater brain entry of peptides (Alkhalifa et al. 2023; Chen et al. 2023). However, it would be of significant benefit to deliver therapeutically-relevant concentrations of peptide into the brain at lower peripheral doses and in particular before disease advanced to a stage where the BBB becomes compromised.

Unlike smaller peptides, large and/or structured peptides such as HsTX1[R14A] or ShK-223 cannot be readily modified to promote passive diffusion across cell membranes (e.g. by modulating hydrophobicity/charge or conformational dynamics) (Ramelot et al. 2023). For these peptides, traversal across an intact BBB typically requires active uptake by brain endothelial cells. Approaches targeting uptake receptors expressed on the BBB using endogenous or synthetic ligands have been shown to be effective in delivering large cargoes into the brain via receptor-mediated endocytosis (Anthony et al. 2021). This strategy is being actively pursued in the development of next-generation biologics for AD that incorporate brain-targeting elements, e.g. Roche's trontinemab and AbbVie's ALIA-1758, both of which include a module that binds to the transferrin receptor (TfR).

BBB shuttle peptides are a promising class of ligands that target transporters expressed at the BBB, and include both sequences derived from natural proteins as well as sequences identified through phage display (Prades et al. 2025). Compared to antibody-based shuttles, BBB shuttle peptides are smaller and more straightforward to synthesize and conjugate to cargoes. Here, we focus on two BBB shuttle peptides, selected based on their reported success in improving transport of large cargoes such as proteins, RNA and nanoparticles across the BBB (Prades et al. 2025). MTfpep (DSSHAFTLDELR) is a tryptic peptide fragment

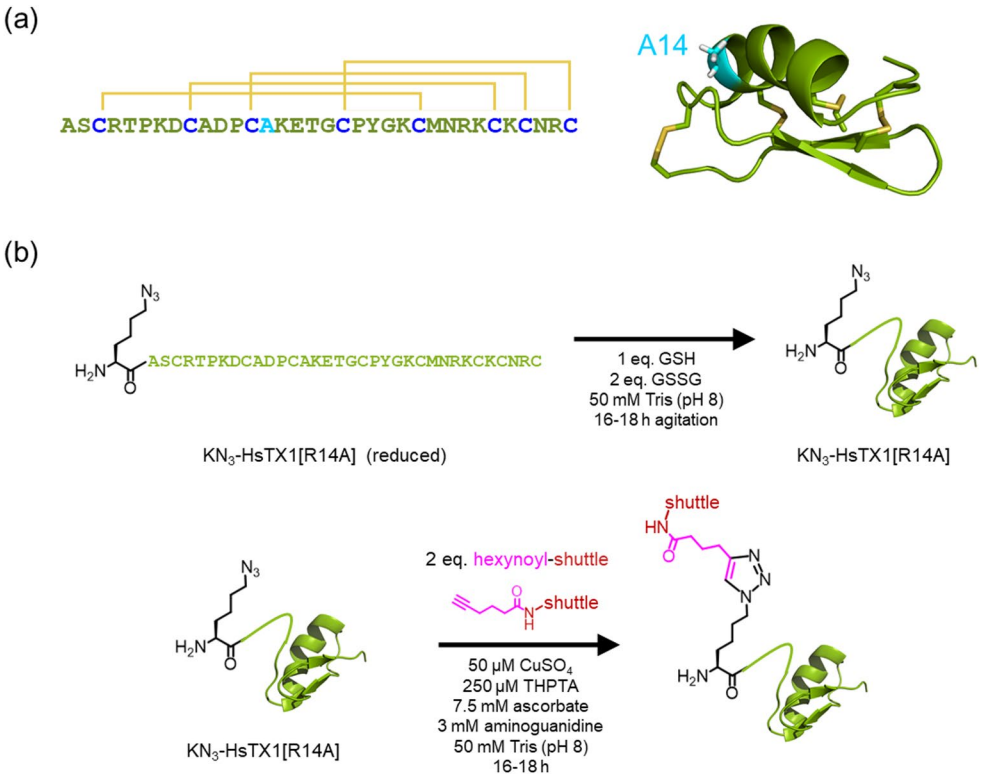

Fig. 1 **a** Sequence of HsTX1[R14A] (with disulfide connectivities indicated) and the solution structure of HsTX1 (PDB 1QUZ), with the disulfides (yellow) and the modelled R14A substitution (cyan) shown as sticks. **b** Reaction scheme for oxidation of KN_3-HsTX1[R14A] and subsequent conjugation of BBB shuttle peptides to HsTX1[R14A]. *GSH* reduced glutathione; *GSSG* oxidized glutathione

derived from melanotransferrin, an endogenous protein ligand of the BBB receptor low-density lipoprotein receptor-related protein 1 (LRP-1), which retains the property of BBB penetration (Singh et al. 2021). It has been shown, either when chemically conjugated or expressed as part of a recombinant protein construct, to enhance the in vivo brain uptake of a mouse IgG1 antibody (~150 kDa) and an engineered protein (interleukin-1 receptor antagonist, IL-1RA) by 4–5 fold at T_{max} (Thom et al. 2018). A fusion protein comprising the human enzyme α-L-iduronidase (IDUA) with MTfpep increased permeation across an in vitro BBB model (hCMEC/D3 monolayer), and improved brain levels of enzyme activity by 4–7 fold compared to unmodified IDUA when delivered as a gene therapy expressed from the liver in IDUA-deficient mice (Jin et al. 2022). An MTfpep-siRNA conjugate (targeting NOX4 in the CNS) administered *i.v.* to healthy mice also showed enhanced (2–3-fold) brain entry compared to siRNA alone (Eyford et al. 2021). Angiopep-2 (TFFYGGSRGKRNNFKTEEY) is a synthetic peptide designed as a chimera of the minimal LRP-interacting domain of the bovine protease inhibitor aprotinin and a homologous sequence in the human amyloid precursor protein (Demeule et al. 2008). It has been used to facilitate BBB transport of diverse cargoes including small molecules (Eiselt et al. 2020; Parrasia et al. 2021; Régina et al. 2008), proteins (Anami et al. 2022; Howell et al. 2024) and nanoparticles (Habib and Singh 2022). Notably, a conjugate of Angiopep-2 with paclitaxel reached Phase II clinical trials for treatment of high-grade glioma, highlighting its translational relevance (Dmello et al. 2024).

In this study, we present a modular approach based on click chemistry for conjugating MTfpep and Angiopep-2 (hereafter MTf and Ang2, respectively) to HsTX1[R14A], and evaluate the ability of these conjugates to cross the BBB in vitro and in vivo.

Results

Synthesis and Biophysical Characterization of Shuttle-HsTX1[R14A] Conjugates

We have shown previously that HsTX1[R14A] and N-terminal conjugates thereof can be synthesized by solid-phase peptide synthesis and folded efficiently (Bergmann et al. 2017; Rashid et al. 2014; Reddiar et al. 2023; Wai et al. 2022). In our initial efforts to create BBB shuttle conjugates of HsTX1[R14A], we synthesized a single polypeptide chain comprising each shuttle sequence N-terminal to HsTX1[R14A], separated by a 3-residue linker (-GSG-). However, the yields of the reduced linear peptide were low, likely due to the length of the peptide (49 residues for MTfpep- and 56 residues for Ang2-HsTX1[R14A]) and cumulative efficiency losses. Moreover, even after HPLC purification of reduced MTf- and Ang2-HsTX1[R14A], oxidative refolding proceeded with poor yields. We therefore

adopted an alternative, modular approach to BBB shuttle attachment using the copper-catalyzed azide–alkyne cycloaddition (CuAAC) (Rostovtsev et al. 2002; Tornøe et al. 2002), as illustrated in Fig. 1. First, HsTX1[R14A] was functionalized by extension of the N-terminus with Nε-azidolysine, and this precursor peptide (hereafter KN_3-HsTX1[R14A]) folded readily under the same oxidative conditions as for HsTX1[R14A] (Fig. S1). Each BBB shuttle was separately synthesized and an alkyne moiety introduced at the N-terminus by amide coupling of hexynoic acid, generating Hex-MTf and Hex-Ang2 (Figs. S2–S5). Finally, purified folded KN_3-HsTX1[R14A] was conjugated to either Hex-MTf or Hex-Ang2 via CuAAC to produce MTf-HsTX1[R14A] or Ang2-HsTX1[R41A], with yields of 50–70%. Liquid chromatography–mass spectrometry (LC-MS) analysis of the conjugates showed good agreement between observed and theoretical masses (Figs. S6, S7). Furthermore, the dispersion of peaks in the amide-aromatic region of the ^{1}H NMR spectra indicated that the conjugates retained the same overall fold as HsTX1[R14A] (Fig. 2). This also validates that any potential reduction of disulfide bonds in HsTX1[R14A] by sodium ascorbate, which is used in CuAAC to reduce Cu(II) to the catalytic Cu(I) species, was reversible upon its removal by HPLC.

Both shuttle-HsTX1[R14A] conjugates were tested for the inhibition of the whole-cell $K_V1.3$ current using patch-clamp electrophysiology. MTf-HsTX1[R14A] and Ang2-HsTX1[R14A] blocked $K_V1.3$ with IC_{50} values of 0.8 and 1.4 nM, respectively (Fig. 3), corresponding to ~20- and 30-fold losses of activity [HsTX1[R14A] $K_V1.3$ IC_{50} ~45 pM (Rashid et al. 2014)], and comparable to other N-terminal modifications of HsTX1[R14A] (Wai et al. 2022).

Development of LCMS/MS Assay to Quantify Peptides in Plasma and Brain

LC-MS/MS assays were developed to quantify HsTX1[R14A], MTf-HsTX1[R14A] and Ang2-HsTX1[R14A] (Supplementary Table S1). However, the largest peak area of transitions identified for Ang2-HsTX1[R14A] was only ~ 10% that of HsTX1[R14A] or MTf-HsTX1[R14A] at 10-fold higher loading (Supplementary Table S2). As the analytical sensitivity of LC-MS/MS detection of Ang2-HsTX1[R14A] was insufficient to quantify the peptide in both in vitro or in vivo permeability assays under the conditions tested, no further quantification of this analogue was conducted.

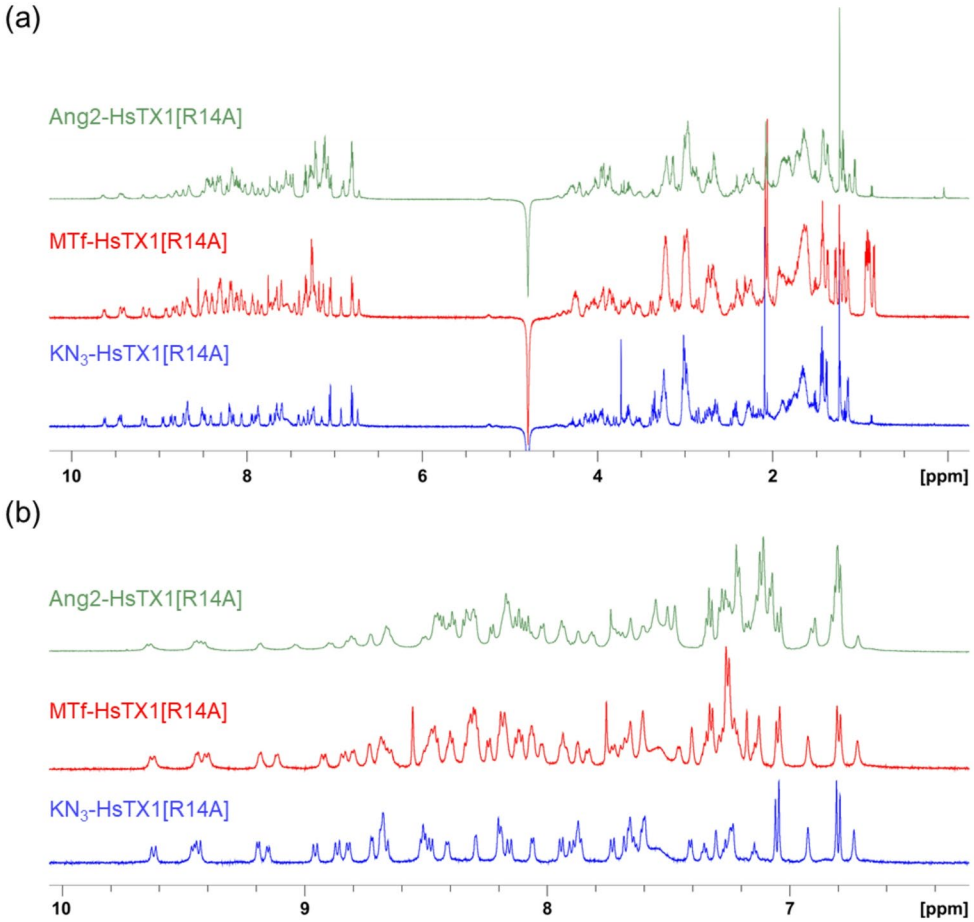

Fig. 2 **a** One-dimensional ^{1}H NMR spectra of KN_3-HsTX1[R14A] (blue), MTf-HsTX1[R14A] (red) and Ang2-HsTX1[R14A] (green) acquired at 600 MHz and 298 K in 95% H_2O/5% ^2H_2O (KN_3-, pH 4.0; MTF-, pH 3.8; Ang2-, pH 4.3). **b** Expanded amide-aromatic region of spectra in (**a**)

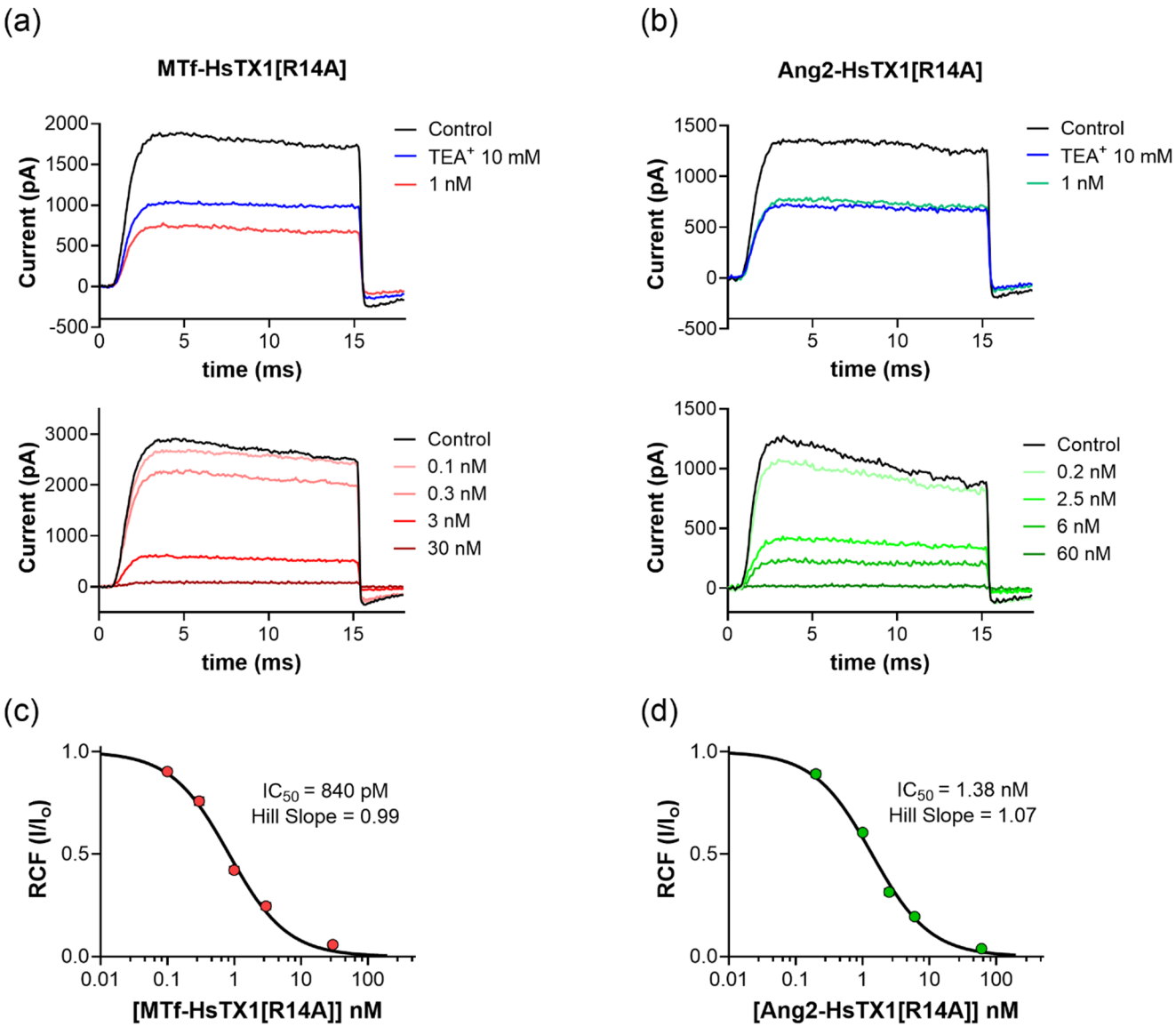

Fig. 3 Electrophysiology assays. **a**, **b** Whole-cell $K_V1.3$ currents were recorded in an activated human T lymphocyte by applying 15-ms-long depolarization pulses to +50 mV from a holding potential of −120 mV every 15 s. Representative current traces show the K^+ current in control solution (black), at steady-state block in the presence of 10 mM TEA^+: tetraethylammonium (blue) as a perfusion control and at equilibrium block in the presence of different concentrations (as indicated in the panels) of **a** MTf-HsTX1[R14A] (red) or **b** Ang2-HsTX1[R14A] (green). **c**, **d** Concentration-response curves of **c** MTf-HsTX1[R14A] or **d** Ang2-HsTX1[R14A] against $K_V1.3$. Remaining current fractions ($RCF = I/I_0$, where I_0 and I are the peak currents in the absence and presence of the indicated concentration of the peptides, respectively) were plotted as a function of peptide concentration. Data were fitted to the Hill equation (see Experimental Procedures) with parameters IC_{50} and H indicated in the panels. Error bars indicate SEM, $n \geq 3$

LCMS/MS assays were validated for HsTX1[R14A] and MTf-HsTX1[R14A] in the assay buffer used for in vitro studies. Analyses of HsTX1[R14A] and MTf-HsTX1[R14A] analogues were precise and accurate from 31 to 1000 nM (Figs. S8A, S8B), with quality control (QC) replicates within this range having a precision < 20% and an accuracy of 80–120% at all concentrations tested (Table 1). In addition, LCMS/MS assays were developed to quantify MTf-HsTX1[R14A] extracted from both mouse plasma and brain homogenate. As demonstrated in Table 2, the assays were precise and accurate, with a precision < 20% and accuracy of 80–120% at all concentrations tested. The assay in mouse brain homogenate was precise and accurate in the range 7.8–250 pmol/g (Fig. S8C) and the assay in plasma was precise and accurate in the range 7.8–500 nM (Fig. S8D). Representative peaks of MTf-HsTX1[R14A] at the low (8 nM) and high (500 nM) concentrations in plasma are shown in Figs. S8E and S8F, respectively. All details of LC gradients and MS ion transitions are detailed in Supplementary Table S1.

Table 1 Precision and accuracy of peptide quantification by LC-MS/MS in in vitro assay buffer ($n=6$)

[HsTX1[R14A]] (nM)	Precision (%)	Accuracy (%)	[MTf-HsTX1[R14A]] (nM)	Precision (%)	Accuracy (%)
31.25	13	101 ± 13	31.25	8	100 ± 9
125	4	94 ± 4	125	4	98 ± 4
1000	3	95 ± 3	1000	9	101 ± 9

Errors represent S.D.

Table 2 Precision and accuracy of peptide quantification by LC-MS/MS in mouse plasma or brain homogenate ($n=6$)

Plasma			Brain homogenate		
[MTf-HsTX1[R14A]] (nM)	Precision (%)	Accuracy (%)	[MTf-HsTX1[R14A]] (pmol/g)	Precision (%)	Accuracy (%)
7.8	12	100 ± 10	7.8	13	92 ± 15
63	6	97 ± 6	63/g	12	83 ± 11
500	6	90 ± 5	250	5	108 ± 5

Errors represent S.D.

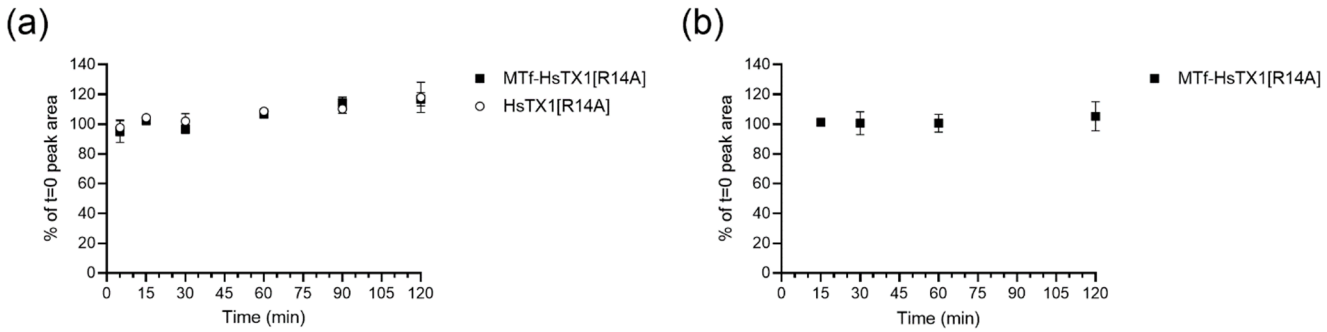

Fig. 4 Stability analysis of **a** HsTX1[R14A] (white circles) and MTf-HsTX1[R14A] (black squares) in in vitro assay buffer at 37 °C, and **b** MTf-HsTX1[R14A] in mouse plasma at 37 °C. Values are percentage LC peak area at the respective timepoints compared to the peak area of the sample taken at the beginning of the study (i.e. t = 0) ($n=3$ per timepoint). Error bars represent S.D. Representative LC-MS/MS peaks of MTf-HsTX1[R14A] in plasma at 0 and 120 min are shown in Fig. S9

Stability of BBB-Shuttle Analogues

Stability analyses were conducted for HsTX1[R14A] and MTf-HsTX1[R14A] in an in vitro assay buffer and for MTf-HsTX1[R14A] in mouse plasma at 37 °C. No degradation was observed for either analogue in any of the solutions tested across the 2 h timeframe analyzed (Fig. 4). We have previously shown that HsTX1[R14A] is stable for >4 h in mouse plasma (unpublished data).

In Vitro Transport of HsTX1[R14A] and MTf-HsTX1[R14A

The permeability of MTf-HsTX1[R14A] compared to HsTX1[R14A] was measured in two in vitro models of the BBB. Permeability across a confluent monolayer of primary mouse brain endothelial cells was evaluated by loading donor chambers with 10 µM peptide, and the concentration transferred across the cell layer to the acceptor chamber measured over a 120 min period. Neither analogue was detected in the acceptor chamber at a concentration above the lower limit of quantification (LLQ) at any timepoint, corresponding to <0.3% transfer over this period. Consequently, in this model, we cannot conclude that MTf-HsTX1[R14A] had increased permeability relative to HsTX1[R14A] as neither peptide was detectable in the acceptor chamber. We further assessed the permeability of both peptides in an immortalized human endothelial brain endothelial (hCMEC/D3) cell model, with a donor chamber concentration of 20 µM. Permeability into the acceptor chamber was low for both analogues, reaching transfer percentages of ~1% over 120 min with no significant difference in the calculated permeability coefficient values ($P_{app} \sim 2E^{-6}$ cm/min) between MTf-HsTX1[R14A] and HsTX1[R14A] (Fig. 5).

In Vivo Plasma and Brain Exposure

C57BL/6 mice were dosed with MTf-HsTX1[R14A] *i.v.* at a dose of 4 mg/kg, and brain and plasma samples taken over a 2-h period (15, 30, 60, 90, 120 min). The plasma and brain concentrations of MTf-HsTX1[R14A] were determined using our validated LC-MS/MS assay. The plasma concentrations of MTf-HsTX1[R14A] are depicted in Fig. 6. As reported in our previous studies (Reddiar et al. 2021), the concentration of HsTX1[R14A] in the brain of C57BL/6 mice was below the LLQ of 15 pmol/g over

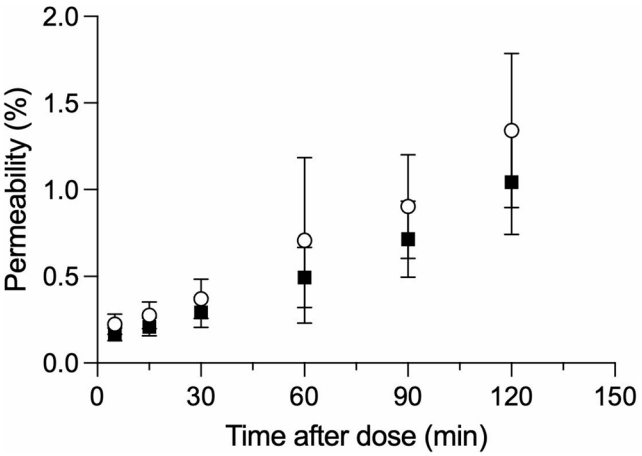

Fig. 5 Permeability of HsTX1[R14A] (white circles) or MTf-HsTX1[R14A] (black squares) across immortalized human brain endothelial (hCMEC/D3) cells. Permeability is defined as percentage concentration in acceptor chamber compared to the concentration present in the donor chamber at timepoint 0 min ($n=4$ per timepoint). Error bars represent S.D

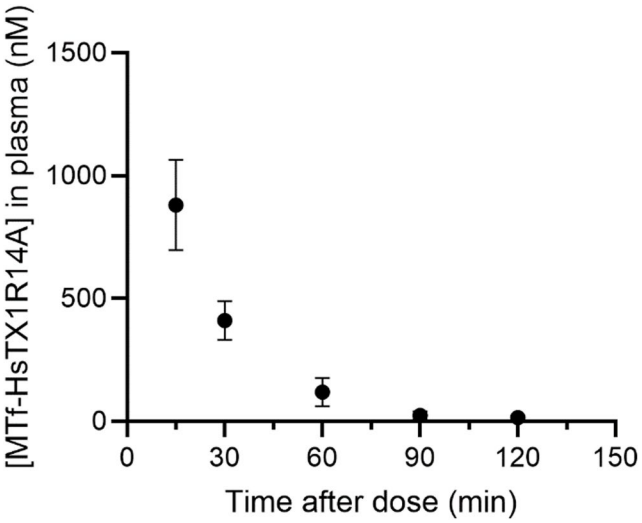

Fig. 6 Plasma concentrations of MTf-HsTX1[R14A] in C57BL/6 mice following intravenous administration at a dose of 4 mg/kg ($n=3$/timepoint). Error bars represent S.D

a 2 h dosing period. In the present study, the concentration of MTf-HsTX1[R14A] in the brain of C57BL/6 mice was below the LLQ of 8 pmol/g over a 2 h dosing period. Therefore, there is no evidence from the present study that MTf-HsTX1[R14A] penetrated the BBB in the mouse model tested at the dose and route of administration analyzed.

Discussion

Peptides are a growing class of therapeutics, with superior potency and selectivity for their targets compared to small molecules, as well as ease of production compared with antibodies (Gare et al. 2025; Muttenthaler et al. 2021; Pennington et al. 2018). However, their therapeutic potential in the CNS is yet to be fully realised, owing to the fact that most peptides (particularly those that are large and structured) are unable to cross the intact BBB. Specific ligands targeting endogenous BBB transport pathways represent one strategy to deliver peptides into the brain.

In the present study, we synthesized and characterized conjugates of the $K_V1.3$-blocking peptide HsTX1[R14A] with the BBB shuttle peptides MTfpep and Angiopep-2, which have been reported to enhance brain delivery of large cargoes in previous studies (Anami et al. 2022; Eyford et al. 2021; Jin et al. 2022; Régina et al. 2008; Thom et al. 2018). We developed LC-MS/MS assays to quantify HsTX1[R14A] and MTf-HsTX1[R14A] in the in vitro assay buffer, mouse plasma and brain homogenate. These methods were precise and accurate to a LLQ of 8 nM (or equivalent), which was sufficient for the assessment of in vivo and in vitro BBB permeability. However, despite the sensitivity of the quantifications of HsTX1[R14A] and MTf-HsTX1[R14A] and the stability of these analogues under the experimental conditions analyzed, neither peptide could be detected in the acceptor chamber in in vitro BBB models using either primary mouse endothelial cells or the hCMEC/D3 cell line. Consistent with this, in vivo studies did not show detectable brain concentrations of MTf-HsTX1[R14A], suggesting that this shuttle peptide did not significantly facilitate the traversal of HsTX1[R14A] across the BBB.

The analytical sensitivity of LC-MS/MS detection of Ang2-HsTX1[R14A] was insufficient to quantify the peptide in our in vitro or in vivo permeability assays under the conditions tested, so no further evaluation of this analogue was conducted. The reasons for the low sensitivity of the analytical method to quantify Ang2-HsTX1[R14A] compared to the other compounds were not ascertained in the current study. The physicochemical properties of the compound may require different sample preparation or LC-MS/MS methods or instrumentation to achieve the required sensitivity (Ewles and Goodwin 2011; Hsieh et al. 2013). Alternatively, bottom-up proteomic approaches utilising trypsin digestion prior to LC/MS quantification could be utilised to establish an analytical method with greater sensitivity. However, we did not pursue such approaches as, in preliminary experiments in mice, Ang2-HsTX1[R14A] at 4 mg/kg *i.v.* produced some adverse effects, and therefore no further work was undertaken with this analogue.

One possible explanation for the lack of BBB traversal of MTf-HsTX1[R14A] is that the conjugation to HsTX1[R14A] compromises the ability of MTfpep to bind to its cognate receptor LRP-1. However, this is unlikely given that successful in vivo BBB traversal has been reported for shuttle-cargo constructs that utilise different attachment points on

the shuttle peptides, for example conjugation of MTfpep via a C-terminal PEG_4-maleimide linker to mAbs (Thom et al. 2018), and recombinant expression of N- and C-terminal fusions of MTfpep to the IDUA enzyme via an $(EAAAK)_3$ linker (Jin et al. 2022).

Several peptidic GLP-1/GIP receptor agonists are currently in Phase II/III clinical trials for AD and PD (Hölscher 2024). Although there is considerable functional evidence to suggest that these peptides act in the CNS, it is less clear that they directly cross the intact BBB, and it has been suggested that they exert their effects via accumulation in specific brain regions known to have a 'leaky' BBB (Salameh et al. 2020). Nerinetide, comprising the cell-penetrating peptide TAT and a 9-residue peptide that blocks a protein-protein interaction to reduce CNS excitotoxicity, is in Phase III clinical trials for acute ischaemic stroke (Hill et al. 2020, 2025). Brain uptake of nerinetide after intravenous administration in mice has been observed, although it has broad biodistribution as TAT does not specifically target the BBB (Kristensen et al. 2020). Intranasal delivery has the potential to deliver peptides into the brain through the olfactory epithelium, thus bypassing the BBB as well as systemic circulation. Much work on intranasal peptide delivery has focused on a handful of peptide cargoes (e.g. insulin, oxytocin) for various CNS indications, with some evidence of efficacy in clinical trials (Bose et al. 2022). Although promising, the broader applicability to other peptides remains to be established, as some cargoes require conjugation or formulation with cell-penetrating peptides and other carriers to promote cell membrane traversal, and in many cases show limited distribution in the brain beyond the olfactory bulb (Meredith et al. 2015; Mittal and Yadav 2025; Schmidt et al. 2025).

Given the failure of MTf-HsTX1[R14A] to show enhanced BBB transport in the current study, future studies will investigate these additional possibilities for improving brain delivery of HsTX1[R14A], facilitated by the conjugation and quantification methods developed in this study. Our results illustrate that, despite reports of successful brain delivery of macromolecules by MTfpep, its effectiveness in promoting brain uptake is not universal.

Experimental Procedures

Peptide Synthesis

All peptides were synthesized using an Fmoc/tBu protection strategy on Rink amide resin (0.68 meq/g, 100–200 mesh). All Fmoc-amino acids were sourced from Chem-Impex (Wood Dale IL, USA), as follows: Ala, Cys(Trt), Asp(OtBu), Glu(OtBu), Gly, His(Trt), Leu, Lys(Boc), $Lys(N_3)$, Met, Phe, Pro, Ser(tBu), Thr(tBu), Tyr(tBu). 5-hexynoic acid was purchased from Combi-Blocks (San Diego CA, USA).

Rink amide resin was swelled for 10 min in N, N-dimethylformamide (DMF). A PS3 peptide synthesizer (Gyros Protein Technologies, Uppsala, Sweden) was used to assemble linear peptide chains by iteration of the following steps: deprotection with 20% (v/v) piperidine in DMF (2 × 5 min); DMF wash (3×); agitation for 50 min in activated amino acid solution comprising Fmoc-amino acid (3 eq.) and O-(1*H*-6-chlorobenzotriazole-1-yl)-1,1,3,3-tetramethyluronium hexafluorophosphate (HCTU, 3 eq.) in 7% (v/v) N, N-diisopropylethylamine (DIPEA) in DMF; DMF wash (3×). 5-hexynoic acid was manually conjugated to each shuttle peptide after the final Fmoc deprotection step, under the same conditions used for amino acid coupling. The completed peptide resins were washed with DMF (3×), methanol (3×) and diethyl ether (3×), then dried using a vacuum pump.

A cleavage solution comprising 85% (v/v) trifluoroacetic acid (TFA), 5% H_2O, 5% thioanisole, 2.5% triisopropylsilane (TIPS) and 2.5% ethane-1,2-dithiol (EDT) was used to remove sidechain protecting groups and cleave the peptide from the resin. The cleavage cocktail was incubated with the resin for 2 h with agitation at ambient temperature (note that longer incubation times led to increased reduction of the azide to the primary amine). The resin was removed from the mixture by filtration, and TFA was evaporated using a nitrogen stream, followed by precipitation of the peptide with excess cold diethyl ether. The peptide was collected by centrifugation (3000×*g*, 4 min) and the pellet washed again by resuspension in ether followed by centrifugation. The final crude material was dissolved in 50% H_2O/50% acetonitrile (ACN) and lyophilized.

Reversed-Phase High-Performance Liquid Chromatography

Crude peptides were resuspended in 95% buffer A (0.1% v/v TFA in H_2O)/5% buffer B (0.1% v/v TFA in ACN), then filtered using a 0.22 µm syringe filter. Samples were separated using a Vydac C_{18} reversed-phase high-performance liquid chromatography (RP-HPLC) column (250 × 10 mm, 10 µm) operated on an Agilent 1260 Infinity II liquid chromatography system. The column was eluted at a flow rate of 4 mL/min using linear gradients as follows: KN_3-HsTX1[R14A] (reduced), 15–30% buffer B over 15 min; Hex-MTf, and Hex-Ang2, 15–45% buffer B over 30 min. Collected fractions were analyzed by liquid chromatography-mass spectroscopy (LC-MS) for identity and purity on a Phenomenex Luna $C_8(2)$ reverse-phase column (100 Å, 3 µm, 100 × 2.0 mm) fitted on a Shimadzu 2020 LC-MS, using a flow rate of 0.2 mL/min and a gradient of 0–60% B

(buffer A: 0.05% v/v TFA in H_2O; buffer B: 0.05% v/v TFA in ACN) over 15 min unless otherwise stated. Fractions containing pure peptide with the correct mass were lyophilized and stored at -20 °C.

Oxidative Refolding of Peptides

HPLC-purified KN_3-HsTX1[R14A] (reduced) was dissolved (1–2 mg/mL) in 50 mM Tris pH 8 containing reduced glutathione (1 eq. relative to peptide) and oxidized glutathione (2 eq.), and air oxidized overnight with gentle agitation. The reaction mixture was purified by RP-HPLC as described above, using a linear gradient of 15–23% buffer B over 16 min at a flow rate of 4 mL/min, and fractions containing pure oxidized KN_3-HsTX1[R14A] were lyophilized.

Copper-Catalyzed Azide–Alkyne Cycloaddition (CuAAC)

CuAAC was conducted under conditions adapted for bioconjugation (Hong et al. 2009). Purified oxidized KN_3-HsTX1[R14A] was dissolved in 50 mM Tris (pH 8) to a final concentration of 0.1–0.3 mM, and 2 eq. of the alkyne-BBB shuttle and aminoguanidine (3 mM) was added. Tris(3-hydroxypropyltriazolylmethyl)amine (THPTA) was pre-combined with $CuSO_4$ in a 5:1 molar ratio before addition to the reaction mixture. Finally, sodium ascorbate (5–7.5 mM) was added, the reaction vessel sealed with parafilm and incubated at ambient temperature overnight. Peptides were purified by RP-HPLC using gradients as follows: MTf-HsTX1[R14A], 17–32% buffer B over 30 min; Ang2-HsTX1[R14A], 20–35% buffer B over 30 min.

Nuclear Magnetic Resonance (NMR) Spectroscopy

Purified peptides (0.1–0.5 mg) were dissolved in 5% ^2H_2O in MilliQ water and the pH measured. One-dimensional ^1H NMR spectra were recorded on a Bruker Avance III 600 MHz spectrometer at 298 K. ^1H chemical shifts were referenced to dioxane (at 3.75 ppm). Spectra were processed and analyzed in Topspin (version 4.5.0).

Patch-Clamp Electrophysiology Assays

To obtain human T lymphocytes, heparinized human peripheral venous blood was drawn from healthy volunteers. Mononuclear cells were separated using Histopaque-1077 (Sigma-Aldrich) separation method following approval from the Ethical Committee of University of Debrecen, (DE RKEB/IKEB 6627-2023). Cells were cultured (density 5×10^5 cells per mL) in Roswell Park Memorial Institute (RPMI) 1640 medium (Gibco) supplemented with 10% FBS, 2 mM L-glutamine and 100 µg/mL streptomycin and 100 U/mL penicillin-g in a humidified incubator at 37 °C and 5% CO_2 for 3–6 days. Phytohemagglutinin A (PHA, Sigma-Aldrich) was also added at a concentration of 2, 5, and 10 µg/mL to activate the T lymphocytes and boost $K_V1.3$ expression. Patch-clamp experiments were performed after 3–6 days of activation.

All measurements were performed using an Axon MultiClamp700B amplifier connected to a personal computer with Axon Digidata 1440 A data acquisition hardware and for data acquisition, Clampex 10.7 software was used (Molecular Devices, Sunnyvale, CA). Whole-cell currents were recorded in voltage-clamp mode following the standard protocols as described previously (Bartok et al. 2015; Naseem et al. 2022). Micropipettes were made from GC150F-7.5 borosilicate capillaries (Harvard Apparatus Co., Holliston, MA, USA) using a Sutter P-1000 puller with tip resistance generally ranging from 3 to 6 MΩ in the bath solution. To evoke the $K_V1.3$ currents in activated T lymphocytes, 15-ms-long voltage pulses to +50 mV from a holding potential of −120 mV were applied every 15 s. All recordings were carried out at room temperature (20–25 °C). Control and test solutions were perfused to the cells via a gravity-driven micro-perfusion system and AutoMate Perfusion Pencil Multi-Barrel Manifold Tip (AutoMate Scientific, Berkeley, CA, USA), and the excess bath solution was continuously removed from recording chamber using vacuum suction. The complete exchange of solution in the bath chamber i.e., the proper operation of the perfusion apparatus was confirmed frequently using 10 mM TEA^+, a reversible inhibitor of $K_V1.3$, as positive control at a concentration equivalent to its IC_{50} value.

The bath (extracellular) solution consisted of (in mM) 145 NaCl, 5 KCl, 2.5 $CaCl_2$, 1 $MgCl_2$, 5.5 glucose, and 10 HEPES, pH 7.35. Equimolar substitution of Na^+ for tetraethylammonium–Cl was used in TEA^+-containing positive control solution. The measured osmolarity of the bath solution was between 302 and 308 mOsM. To prevent peptide adsorption to the plastic surfaces of the perfusion system bath solutions were supplemented with 0.1 mg/mL bovine serum albumin (BSA, Sigma-Aldrich, Hungary). The composition of internal solution was (in mM) 140 KF, 2 $MgCl_2$, 1 $CaCl_2$, 10 HEPES and 11 EGTA, pH 7.22. The measured osmolarity of internal solutions was ~ 295 mOsm/L.

Data were analysed using pClamp 10.7 software package (Molecular Devices, Sunnyvale, CA). The remaining current fraction (RCF) were fitted using the Hill equation:

$$RCF = \frac{I}{I_0} = \frac{{IC_{50}}^H}{{IC_{50}}^H + [\text{peptide}]^H},$$

where I and I_0 are the peak currents measured in the presence and absence of peptide, respectively (giving the ratio RCF, remaining current fraction), IC_{50} is the concentration of the peptide that gives 50% block, [peptide] is the concentration of peptide (M), and H is the Hill coefficient.

Buffer and Plasma Stability Assays

The stability of HsTX1[R14A] or MTf-HsTX1[R14A] was analyzed in Hanks Balanced Salt Solution (ThermoFisher Scientific, Rockport, IL) containing 10 mM N-2-hydroxyethylpiperazine-N-2-ethane sulfonic acid (HEPES; Sigma-Aldrich, St Louis, MO) at pH 7.4, hereafter referred to as HBSS. HBSS was pre-warmed at 37 °C and 20 µM of either HsTX1[R14A] or MTf-HsTX1[R14A] was added to three separate vial replicates, which were maintained at 37 °C for the duration of the study. Samples were taken at 0, 5, 15, 30, 60, 90 and 120 min timepoints. The stability of MTf-HsTX1[R14A] was also assessed in the plasma of adult C57BL/6 mice. Plasma was aliquoted to three separate vials and pre-warmed at 37 °C. MTf-HsTX1[R14A] was added to the plasma at 800 nM. Samples were taken at 0, 15, 30, 60, and 120 min.

In Vitro BBB Model

hCMEC/D3 cells were obtained from Merck Millipore and utilized between passages 5–11. Primary brain microvascular endothelial cells were isolated from C57BL/6 mice (Monash Institute of Pharmaceutical Sciences Ethics application MIPS 29011) using a magnetic activated cell sorting approach with a CD31 antibody, as previously described in detail (Runwal et al. 2025). hCMEC/D3 cells were seeded onto Transwell (0.4 µm, polyester) inserts within a 24-well plate coated with rat-tail collagen Type I (100 µg/mL). Primary mouse brain microvascular endothelial cells were seeded onto Transwell (0.4 µm, polyester) inserts within a 24-well plate coated with 100 µL of solution containing 40% (v/v) Type IV collagen, 10% (v/v) fibronectin and 50% (v/v) UltraPure™ distilled water. hCMEC/D3 cells were used for permeability studies 7 days post-seeding. For primary mouse brain endothelial cells, permeability studies were commenced when the calculated transendothelial electrical resistance (TEER) values reached greater than 150 Ω.cm^2, which typically took 6 to 7 days.

Plates were maintained at 37 °C for the duration of the permeability study on the THERMOstar (BMG Labtech, Ortenberg, Germany). HsTX1[R14A] or MTf-HsTX1[R14A] were added to the donor chamber at 10 and 20 µM for primary and hCMEC/D3 cells, respectively ($n=4$). Samples were taken from the donor chamber at the start of the experiment and from the acceptor chamber at 5, 15, 30, 60, 90 and 120 min, and replaced with equal volumes of transport buffer in the acceptor chamber. Concentrations were corrected to account for this dilution. P_{app} was calculated by the following equation:

$$P_{app} = (dQ/dt)/(C_0 \times A),$$

where dQ/dt is the rate that the compound appears in the acceptor chamber, C_0 is the initial concentration of compound in the donor chamber, and A is the 0.33 cm^2 cross-sectional area of the Transwell membrane.

Mouse Brain and Plasma Exposure

Animal experiments were conducted according to protocols approved by the Monash Institute of Pharmaceutical Sciences Animal Ethics Committee (ethics submission #28460) and performed in accordance with the National Health and Medical Research Council Guidelines for the care and use of animals for scientific purposes. Adult C57BL/6 mice (8–12 weeks) were intravenously dosed with 4 mg/kg MTf-HsTX1[R14A] dissolved in phosphate buffered saline. At designated timepoints (5, 15, 30, 60, 90–120 min), mice were anaesthetised with isoflurane in oxygen (1–5%). Cardiac puncture was performed to obtain blood in tubes containing lithium heparin (Sarstedt, Nümbrecht, Germany). Tubes were centrifuged at 2000 rcf for 5 min and the plasma supernatant was collected and placed on dry ice. Whole brains were removed and placed on dry ice. All samples were stored at − 20 °C until analysis.

Peptide Extraction and LC-MS/MS Quantification

Samples from HsTX1[R14A] and MTf-HsTX1[R14A] in vitro assays were diluted as two parts sample to one part methanol, for a final concentration of 33% (v/v) methanol. Donor chamber samples were diluted one part to 49 parts in HBSS before adding 25 parts methanol. Standards were produced by dissolving peptide in water to make a series of spike standards. Spike standards were added as a one part to nine parts in HBSS in vitro assay solution, before adding five parts methanol for a final concentration of 33% (v/v) methanol.

MTf-HsTX1[R14A] was extracted from plasma samples and standards. Plasma was obtained from dosed mice or produced as spiked standards in plasma obtained from untreated mice. Standards were prepared via serially diluted spiking solutions that were spiked as one part to 99 parts plasma. Blank plasma was also included as a control. Plasma samples and standards (100 µL) were diluted with LC-MS/MS grade MilliQ water (500 µL). Waters tC18 Cartridges (WAT054960; MA, USA) were attached to a Waters extraction manifold (WAT200607) and vacuum pressure set at ~ 1 PSI. Cartridges were primed by allowing 500 µL of

methanol to flow through, followed by 500 µL of LC-MS/MS grade MilliQ water. The sample or standard was allowed to flow through, followed by a wash with 500 µL 5% methanol. A tube was placed under the cartridge and elution was performed with 500 µL of 99% methanol, 1% formic acid. Samples were placed in a Biotage (Uppsala, Sweden) TurboVap (40 °C water bath, 1.5 mL/min flow rate) and evaporated to dryness under nitrogen flow. Samples were reconstituted in 50 µL of 50% methanol.

MTf-HsTX1[R14A] was extracted from brain samples and standards. Brains were obtained from dosed mice or produced as spiked standards in brain obtained from untreated mice. Standards were prepared by serially diluting spiking solution and homogenising 300 mg of mouse brain in 600 µL of MilliQ water before spiking 3 µL of spiking solution into each sample. A blank plasma sample was also included as a control. Waters PRiME HLB 3 cc cartridge (Catalogue #186008056) were attached to a Waters extraction manifold and vacuum pressure set at ~1 psi. Cartridges were primed by allowing 1 mL of methanol to flow through, followed by 1 ml of LC-MS/MS grade MilliQ water. Brain samples and standards (600 µL homogenates from 300 mg of brain) were allowed to flow through, followed by a wash of 1 mL 5% methanol. A tube was placed under the cartridge and elution was performed with 300 µL of 70% methanol, 1% formic acid. Samples were placed in a Biotage (Uppsala, Sweden) TurboVap (40 °C water bath, 1 mL/min flow rate) and evaporated to dryness under nitrogen flow. Samples were reconstituted in 50 µL 50% methanol.

All samples were analyzed on a Shimadzu (Kyoto, Japan) 8060 tandem quadrupole mass spectrometer using a Phenomenex (CA, USA) Kinetex 2.6 µm polar C18 LC column (100 × 2.1 mm, 100 Å pore size) with Security Guard Ultra cartridge UHPLC polar C18 column (2.1 mm internal diameter). Mobile phases were A: MilliQ water (0.1% formic acid) and B: 100% methanol. Injection volumes were 6 µL, autosampler was held at 4 °C, column oven was held at 40 °C and flow rate was set at 0.5 mL/min. Gradient methods and quantifying and qualifying transitions are listed in Supplementary Table S1.

Linear ranges of each peptide in HBSS were tested at 31.25, 62.5, 125, 250, 500 and 1000 nM. Precision and accuracy were tested by the preparation of six separate replicates at 31.25, 125 and 1000 nM. Peak areas were converted to nM via a $1/x^2$ weighted linear equation based on the standards. Precision was determined as the standard deviation of the concentrations calculated for each replicate divided by the average of the concentrations calculated for each replicate. The accuracy was determined by comparing the calculated concentration for each replicate against the theoretical concentration and taking an average of that value for all replicates. Precision values < 13% and accuracy values between 90 and 110% were identified for both peptides at all concentrations tested (Table 1). Linear ranges of MTf-HsTX1[R14A] were 7.8, 15.6, 31.25, 62.5, 125 and 250 nM in mouse brain and 7.8, 15.6, 31.25, 62.5, 125, 250 nM in plasma. Precision and accuracy were determined in the same manner as detailed for HBSS above. Precision values < 13% and accuracy values between 80 and 110% were identified for both peptides at all concentrations tested (Table 2).

Supplementary Information The online version contains supplementary material available at https://doi.org/10.1007/s10989-026-10810-w.

Acknowledgements We thank Dr Ryan Keenan for helpful discussions and for reviewing the manuscript draft.

Author Contributions DCCW, JAN, DIF and RSN conceived the project, DCCW synthesized and characterized peptides, LMK undertook LC-MS assay development, in vitro stability and pharmacokinetic studies, EK and PR conducted in vitro BBB permeation assays, MUN and GP undertook the electrophysiology assays. All authors contributed to writing the manuscript. DCCW and LMK are equal first authors.

Funding Open Access funding enabled and organized by CAUL and its Member Institutions. The following grants supported part of this work: Dementia Australia 2022 Bondi2Berry Project Grant, Parkinson's Foundation 2023 Bill and Amy Gurley Impact Award (PF-IMP-1148847), Project 2024-1.2.3-HU-RIZONT-2024-00099 provided by the Ministry of Culture and Innovation of Hungary from the National Research, Development, and Innovation Fund, financed under the 2024-1.2.3-HU-RIZONT funding scheme.

Data Availability All data supporting the findings of this study are available within the paper and its Supplementary Information.

Declarations

Conflict of interest The authors have no relevant financial or non-financial interests to disclose.

References

Alkhalifa AE, Al-Ghraiybah NF, Odum J, Shunnarah JG, Austin N, Kaddoumi A (2023) Blood–brain barrier breakdown in

Alzheimer's disease: mechanisms and targeted strategies. Int J Mol Sci 24:16288. https://doi.org/10.3390/ijms242216288

Anami Y, Xiong W, Yamaguchi A, Yamazaki CM, Zhang N, An Z et al (2022) Homogeneous antibody–angiopep 2 conjugates for effective brain targeting. RSC Adv 12:3359–3364. https://doi.org/10.1039/d1ra08131d

Anthony DP, Hegde M, Shetty SS, Rafic T, Mutalik S, Rao BSS (2021) Targeting receptor-ligand chemistry for drug delivery across blood–brain barrier in brain diseases. Life Sci 274:119326. https://doi.org/10.1016/j.lfs.2021.119326

Bartok A, Fehér K, Bodor A, Rákosi K, Tóth GK, Kövér KE et al (2015) An engineered scorpion toxin analogue with improved K_V1.3 selectivity displays reduced conformational flexibility. Sci Rep 5:18397. https://doi.org/10.1038/srep18397

Bergmann R, Kubeil M, Zarschler K, Chhabra S, Tajhya RB, Beeton C et al (2017) Distribution and kinetics of the K_V1.3-blocking peptide HsTX1[R14A] in experimental rats. Sci Rep 7:3756. https://doi.org/10.1038/s41598-017-03998-x

Bose M, Farias Quipildor G, Ehrlich ME, Salton SR (2022) Intranasal peptide therapeutics: A promising avenue for overcoming the challenges of traditional CNS drug development. Cells 11:3629. https://doi.org/10.3390/cells11223629

Chen Y, He Y, Han J, Wei W, Chen F (2023) Blood–brain barrier dysfunction and Alzheimer's disease: associations, pathogenic mechanisms, and therapeutic potential. Front Aging Neurosci 15:1258640 https://doi.org/10.3389/fnagi.2023.1258640

Demeule M, Régina A, Ché C, Poirier J, Nguyen T, Gabathuler R et al (2008) Identification and design of peptides as a new drug delivery system for the brain. J Pharmacol Exp Ther 324:1064–1072. https://doi.org/10.1124/jpet.107.131318

Di Lucente J, Nguyen HM, Wulff H, Jin L-W, Maezawa I (2018) The voltage-gated potassium channel K_V1.3 is required for microglial pro-inflammatory activation in vivo. Glia 66:1881–1895. https://doi.org/10.1002/glia.23457

Dmello C, Brenner A, Piccioni D, Wen PY, Drappatz J, Mrugala M et al (2024) Phase II trial of blood–brain barrier permeable peptide-paclitaxel conjugate ANG1005 in patients with recurrent high-grade glioma. Neurooncol Adv 6(1):vdae186. https://doi.org/10.1093/noajnl/vdae186

Eiselt É, Otis V, Belleville K, Yang G, Larocque A, Régina A et al (2020) Use of a noninvasive brain-penetrating peptide-drug conjugate strategy to improve the delivery of opioid pain relief medications to the brain. J Pharmacol Exp Ther 374:52–61. https://doi.org/10.1124/jpet.119.263566

Ewles M, Goodwin L (2011) Bioanalytical approaches to analyzing peptides and proteins by LC–MS/MS. Bioanalysis 3:1379–1397. https://doi.org/10.4155/bio.11.112

Eyford BA, Singh CSB, Abraham T, Munro L, Choi KB, Hill T et al (2021) A nanomule peptide carrier delivers siRNA across the intact blood–brain barrier to attenuate ischemic stroke. Front Mol Biosci 8:611367 https://doi.org/10.3389/fmolb.2021.611367

Gare CL, White AM, Malins LR (2025) From lead to market: chemical approaches to transform peptides into therapeutics. Trends Biochem Sci 50:467–480. https://doi.org/10.1016/j.tibs.2025.01.009

Habib S, Singh M (2022) Angiopep-2-modified nanoparticles for brain-directed delivery of therapeutics: a review. Polymers 14:712. https://doi.org/10.3390/polym14040712

Heneka MT, Van Der Flier WM, Jessen F, Hoozemanns J, Thal DR, Boche D et al (2025) Neuroinflammation in Alzheimer disease. Nat Rev Immunol 25:321–352. https://doi.org/10.1038/s41577-024-01104-7

Hill MD, Goyal M, Menon BK, Nogueira RG, Mctaggart RA, Demchuk AM et al (2020) Efficacy and safety of nerinetide for the treatment of acute ischaemic stroke (ESCAPE-NA1): a multicentre, double-blind, randomised controlled trial. Lancet 395:878–887. https://doi.org/10.1016/S0140-6736(20)30258-0

Hill MD, Goyal M, Demchuk AM, Menon BK, Field TS, Guest WC et al (2025) Efficacy and safety of nerinetide in acute ischaemic stroke in patients undergoing endovascular thrombectomy without previous thrombolysis (ESCAPE-NEXT): a multicentre, double-blind, randomised controlled trial. Lancet 405:560–570. https://doi.org/10.1016/S0140-6736(25)00194-1

Hölscher C (2024) Glucagon-like peptide-1 class drugs show clear protective effects in Parkinson's and Alzheimer's disease clinical trials: A revolution in the making? Neuropharmacology 253:109952. https://doi.org/10.1016/j.neuropharm.2024.109952

Hong V, Presolski SI, Ma C, Finn MG (2009) Analysis and optimization of copper-catalyzed azide–alkyne cycloaddition for bioconjugation. Angew Chem Int 48:9879–9883. https://doi.org/10.1002/anie.200905087

Howell RA, Wang S, Khambete M, Mcdonald DM, Spiegel DA (2024) Bifunctional molecules that induce both targeted degradation and transcytosis of extracellular proteins in brain cells. J Am Chem Soc 146:16404–16411. https://doi.org/10.1021/jacs.3c13320

Hsieh EJ, Bereman MS, Durand S, Valaskovic GA, Maccoss MJ (2013) Effects of column and gradient lengths on peak capacity and peptide identification in nanoflow LC-MS/MS of complex proteomic samples. J Am Soc Mass Spectrom 24:148–153. https://doi.org/10.1007/s13361-012-0508-6

Jin L, Zhou Q, Chan H-K, Larson IC, Pennington MW, Morales RV et al (2016) Pulmonary delivery of the K_V1.3-blocking peptide HsTX1[R14A] for the treatment of autoimmune diseases. J Pharm Sci 105:650–656. https://doi.org/10.1016/j.xphs.2015.10.025

Jin X, Su J, Zhao Q, Li R, Xiao J, Zhong X et al (2022) Liver-directed gene therapy corrects neurologic disease in a murine model of mucopolysaccharidosis type I-Hurler. Mol Ther Methods Clin Dev 25:370–381. https://doi.org/10.1016/j.omtm.2022.04.010

Kristensen M, Kucharz K, Felipe Alves Fernandes E, Strømgaard K, Schallburg Nielsen M, Cederberg Helms HC et al (2020) Conjugation of therapeutic PSD-95 inhibitors to the cell-penetrating peptide Tat affects blood–brain barrier adherence, uptake, and permeation. Pharmaceutics 12:661. https://doi.org/10.3390/pharmaceutics12070661

Lebrun B, Romi-Lebrun R, Martin-Eauclaire MF, Yasuda A, Ishiguro M, Oyama Y et al (1997) A four-disulphide-bridged toxin, with high affinity towards voltage-gated K^+ channels, isolated from *Heterometrus spinnifer* (Scorpionidae) venom. Biochem J 328(Pt 1):321–327. https://doi.org/10.1042/bj3280321

Maezawa I, Nguyen HM, Di Lucente J, Jenkins DP, Singh V, Hilt S et al (2017) K_V1.3 Inhibition as a potential microglia-targeted therapy for Alzheimer's disease: preclinical proof of concept. Brain 141:596–612. https://doi.org/10.1093/brain/awx346

Meredith ME, Salameh TS, Banks WA (2015) Intranasal delivery of proteins and peptides in the treatment of neurodegenerative diseases. AAPS J 17:780–787. https://doi.org/10.1208/s12248-015-9719-7

Mittal V, Yadav KS (2025) Optimizing nasal drug delivery for peptides, proteins, and small molecules: strategic use of materials and techniques to target the CNS. Int J Polym Mater Polym Biomater 74:1400–1423. https://doi.org/10.1080/00914037.2024.2443165

Muttenthaler M, King GF, Adams DJ, Alewood PF (2021) Trends in peptide drug discovery. Nat Rev Drug Discov 20:309–325. https://doi.org/10.1038/s41573-020-00135-8

Naseem MU, Carcamo-Noriega E, Beltrán-Vidal J, Borrego J, Szanto TG, Zamudio FZ et al (2022) Cm28, a Scorpion toxin having a unique primary structure, inhibits K_V1.2 and K_V1.3 with high affinity. J Gen Physiol 154:e202213146 https://doi.org/10.1085/jgp.202213146

Norton RS, Chandy KG (2017) Venom-derived peptide inhibitors of voltage-gated potassium channels. Neuropharmacology 127:124–138. https://doi.org/10.1016/j.neuropharm.2017.07.002

Pan Y, Kagawa Y, Sun J, Lucas DSD, Takechi R, Mamo JCL et al (2023) Peripheral administration of the Kv1.3-blocking peptide HsTX1[R14A] improves cognitive performance in senescence accelerated SAMP8 mice. Neurotherapeutics 20:1198–1214. https://doi.org/10.1007/s13311-023-01387-z

Parrasia S, Rossa A, Varanita T, Checchetto V, De Lorenzi R, Zoratti M et al (2021) An Angiopep2-PAPTP construct overcomes the blood–brain barrier. New perspectives against brain tumors. Pharmaceuticals 14:129. https://doi.org/10.3390/ph14020129

Pennington MW, Czerwinski A, Norton RS (2018) Peptide therapeutics from venom: Current status and potential. Bioorg Med Chem 26:2738–2758. https://doi.org/10.1016/j.bmc.2017.09.029

Prades R, Teixidó M, Oller-Salvia B (2025) New trends in brain shuttle peptides. Mol Pharm 22:1100–1109. https://doi.org/10.1021/acs.molpharmaceut.4c01327

Ramelot TA, Palmer J, Montelione GT, Bhardwaj G (2023) Cell-permeable chameleonic peptides: Exploiting conformational dynamics in de novo cyclic peptide design. Curr Opin Struct Biol 80:102603. https://doi.org/10.1016/j.sbi.2023.102603

Ramesha S, Rayaprolu S, Bowen CA, Giver CR, Bitarafan S, Nguyen HM et al (2021) Unique molecular characteristics and microglial origin of K_V1.3 channel–positive brain myeloid cells in Alzheimer's disease. Proc Natl Acad Sci USA 118:e2013545118. https://doi.org/10.1073/pnas.2013545118

Rangaraju S, Gearing M, Jin L-W, Levey A (2015) Potassium channel K_V1.3 is highly expressed by microglia in human Alzheimer's disease. J Alzheimer's Dis 44:797–808. https://doi.org/10.3233/JAD-141704

Rashid MH, Huq R, Tanner MR, Chhabra S, Khoo KK, Estrada R et al (2014) A potent and K_V1.3-selective analogue of the scorpion toxin HsTX1 as a potential therapeutic for autoimmune diseases. Sci Rep 4:4509. https://doi.org/10.1038/srep04509

Reddiar SB, Jin L, Wai DCC, Csoti A, Panyi G, Norton RS et al (2021) Lipopolysaccharide influences the plasma and brain pharmacokinetics of subcutaneously-administered HsTX1[R14A], a K_V1.3-blocking peptide. Toxicon 195:29–36. https://doi.org/10.1016/j.toxicon.2021.03.002

Reddiar SB, De Veer M, Paterson BM, Sepehrizadeh T, Wai DCC, Csoti A et al (2023) A biodistribution study of the radiolabeled K_V1.3-blocking peptide DOTA-HsTX1[R14A] demonstrates brain uptake in a mouse model of neuroinflammation. Mol Pharm 20:255–266. https://doi.org/10.1021/acs.molpharmaceut.2c00614

Régina A, Demeule M, Ché C, Lavallée I, Poirier J, Gabathuler R et al (2008) Antitumour activity of ANG1005, a conjugate between paclitaxel and the new brain delivery vector Angiopep-2. Br J Pharmacol 155:185–197. https://doi.org/10.1038/bjp.2008.260

Rostovtsev VV, Green LG, Fokin VV, Sharpless KB (2002) A stepwise Huisgen cycloaddition process: Copper(I)-catalyzed regioselective ligation of azides and terminal alkynes. Angew Chem Int 41:2596–2599. https://doi.org/10.1002/1521-3773(20020715)41:14%3C2596::AID-ANIE2596%3E3.0.CO;2-4

Runwal P, Pyun J, Newman SA, Mawal C, Bush AI, Koehn LM et al (2025) Ferric ammonium citrate reduces claudin-5 abundance and function in primary mouse brain endothelial cells. Pharm Res 42:319–334. https://doi.org/10.1007/s11095-025-03826-2

Salameh TS, Rhea EM, Talbot K, Banks WA (2020) Brain uptake pharmacokinetics of incretin receptor agonists showing promise as Alzheimer's and Parkinson's disease therapeutics. Biochem Pharmacol 180:114187. https://doi.org/10.1016/j.bcp.2020.114187

Sarkar S, Nguyen HM, Malovic E, Luo J, Langley M, Palanisamy BN et al (2020) K_V1.3 modulates neuroinflammation and neurodegeneration in Parkinson's disease. J Clin Investig 130:4195–4212. https://doi.org/10.1172/JCI136174

Schmidt SE, Joensen G, Sandbjerg C, Thaysen M, Gammelgaard B, Schindowski K et al (2025) The PSD-95 inhibitor NA-1 is delivered to the brain upon nasal administration with uptake into the olfactory bulb improved by co-administration with the cell-penetrating peptides lowPro and Tat. Drug Deliv Transl Res. https://doi.org/10.1007/s13346-025-01842-8

Schmitz A, Sankaranarayanan A, Azam P, Schmidt-Lassen K, Homerick D, Hänsel W et al (2005) Design of PAP-1, a selective small molecule K_V1.3 blocker, for the suppression of effector memory T cells in autoimmune diseases. Mol Pharmacol 68:1254. https://doi.org/10.1124/mol.105.015669

Singh CSB, Eyford BA, Abraham T, Munro L, Choi KB, Okon M et al (2021) Discovery of a highly conserved peptide in the iron transporter melanotransferrin that traverses an intact blood brain barrier and localizes in neural cells. Front Neurosci 15:596976 https://doi.org/10.3389/fnins.2021.596976

Tansey MG, Wallings RL, Houser MC, Herrick MK, Keating CE, Joers V (2022) Inflammation and immune dysfunction in Parkinson disease. Nat Rev Immunol 22:657–673. https://doi.org/10.1038/s41577-022-00684-6

Thom G, Tian M-M, Hatcher JP, Rodrigo N, Burrell M, Gurrell I et al (2018) A peptide derived from melanotransferrin delivers a protein-based interleukin 1 receptor antagonist across the BBB and ameliorates neuropathic pain in a preclinical model. J Cereb Blood Flow Metab 39:2074–2088. https://doi.org/10.1177/0271678X18772998

Tornøe CW, Christensen C, Meldal M (2002) Peptidotriazoles on solid phase: [1,2,3]-triazoles by regiospecific copper(i)-catalyzed 1,3-dipolar cycloadditions of terminal alkynes to azides. J Org Chem 67:3057–3064. https://doi.org/10.1021/jo011148j

Wai DCC, Naseem MU, Mocsár G, Babu Reddiar S, Pan Y, Csoti A et al (2022) A fluorescent peptide toxin for selective visualization of the voltage-gated potassium channel K_V1.3. Bioconjug Chem 33:2197–2212. https://doi.org/10.1021/acs.bioconjchem.2c00436

Zhang W, Xiao D, Mao Q, Xia H (2023) Role of neuroinflammation in neurodegeneration development. Signal Transduct Target Ther 8:267. https://doi.org/10.1038/s41392-023-01486-5